

Full Paper

Characterization of a Unique Co-Crystal of the BACE1 inhibitor Verubecestat and a reaction intermediate: Implications to the Development of a Commercial Manufacturing Process

Laura Artino, Richard J. Varsolona, Andrew P. J. Brunskill, William J Morris, David A. Thaisrivongs, Jacob H Waldman, Thomas W Lyons, and Yanke Xu

Org. Process Res. Dev., **Just Accepted Manuscript** • DOI: 10.1021/acs.oprd.8b00015 • Publication Date (Web): 22 Feb 2018

Downloaded from <http://pubs.acs.org> on February 23, 2018

Just Accepted

“Just Accepted” manuscripts have been peer-reviewed and accepted for publication. They are posted online prior to technical editing, formatting for publication and author proofing. The American Chemical Society provides “Just Accepted” as a service to the research community to expedite the dissemination of scientific material as soon as possible after acceptance. “Just Accepted” manuscripts appear in full in PDF format accompanied by an HTML abstract. “Just Accepted” manuscripts have been fully peer reviewed, but should not be considered the official version of record. They are citable by the Digital Object Identifier (DOI®). “Just Accepted” is an optional service offered to authors. Therefore, the “Just Accepted” Web site may not include all articles that will be published in the journal. After a manuscript is technically edited and formatted, it will be removed from the “Just Accepted” Web site and published as an ASAP article. Note that technical editing may introduce minor changes to the manuscript text and/or graphics which could affect content, and all legal disclaimers and ethical guidelines that apply to the journal pertain. ACS cannot be held responsible for errors or consequences arising from the use of information contained in these “Just Accepted” manuscripts.



1
2
3 Characterization of a Unique Co-Crystal of the BACE1 inhibitor Verubecestat and a reaction
4
5 intermediate: Implications to the Development of a Commercial Manufacturing Process
6
7

8
9 Laura Artino,* Richard Varsolona, Andrew P. J. Brunskill, William J. Morris, David A.

10
11 Thaisrivongs, Jacob H. Waldman, Thomas W. Lyons, and Yanke Xu

12
13 *Department of Process Research and Development, MRL, Merck & Co., Inc., Rahway, NJ 07065*

14
15
16 USA

17
18 laura_artino@merck.com

19
20
21 RECEIVED DATE (will be automatically inserted after manuscript is accepted).

22
23 **Abstract:** Verubecestat is an inhibitor of the beta-site amyloid precursor protein cleaving
24
25 enzyme 1 (BACE1) currently under clinical evaluation for the treatment prodromal Alzheimer's
26
27 disease. This article describes the characterization of a co-crystal composed of an HBr salt of
28
29 verubecestat and a HBr salt of a reaction intermediate as the components. This unique co-crystal
30
31 was formed during a multi-kilogram production batch of verubecestat. The impact of this
32
33 observation is discussed followed by the description of a modified procedure that served to
34
35 prevent the formation of this highly unusual crystalline material.
36
37

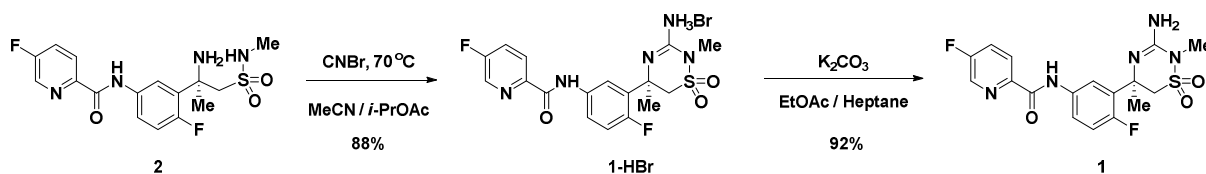
38
39
40 **Keywords:** Co-crystal, reaction intermediate, BACE1 inhibitor, Verubecestat, Alzheimer's
41
42 disease
43
44

45
46
47
48
49
50
51
52
53
54
55
56
57
58
59
60

1
2
3 Alzheimer's disease (AD), the most common form of dementia, is a neurodegenerative disorder
4 that results in the erosion of memory, vocal control, and cognitive skills before ultimately
5
6 resulting in death. There are currently greater than 5.5 million Americans living with AD in
7
8 2017, part of a worldwide total that is estimated to be 47 million.^{1,2} These figures are expected
9
10 to grow, with a projected patient population of over 130 million by 2050. Pharmacological
11
12 intervention is limited to treatments that temporarily address the symptoms of the disease but
13
14 there are currently no disease modifying therapies available to patients. One potential class of
15
16 therapies currently under clinical evaluation are inhibitors of the beta-site amyloid precursor
17
18 protein cleaving enzyme 1 (BACE1), which seek to interrupt the processing of amyloid precursor
19
20 protein (APP) and prevent the formation and deposition of the hallmark amyloid plaques
21
22 between neurons in AD patients.
23
24
25
26
27
28

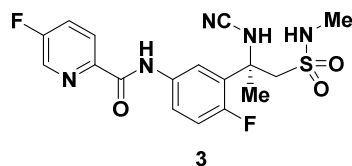
29 Verubecestat (**1**), an inhibitor of BACE1, is currently being evaluated in the clinic for the
30
31 treatment of prodromal Alzheimer's disease.^{3,4} Our laboratories previously disclosed a
32
33 communication describing the development of a commercial manufacturing route to **1** which
34
35 relied on a reactive crystallization to form the 3-amino-1,2,4-thiadiazinene 1,1'-dioxide
36
37 heterocycle of **1**.⁵ In our previous report, amine **2** was condensed with cyanogen bromide (CNBr)
38
39 in the absence of base to yield the HBr salt of verubecestat (**1-HBr**, Scheme 1). Following a salt
40
41 break with K₂CO₃, the active pharmaceutical ingredient (API) was isolated in 81% yield from **2**.
42
43
44
45

46 Scheme 1: Preparation of verubecestat (**1**) via reactive crystallization



The application of the reactive crystallization afforded several advantages from a processing perspective. First, the crystallization of **1-HBr** prevented the overalkylation of **1** by CNBr. (*vide infra*). Second, the reactive crystallization eliminated the need to carry out an aqueous workup and a separate isolation operation as the process afforded a direct isolation of **1-HBr** and providing the product in >99% purity. We successfully demonstrated this reactive crystallization on an initial multi-kilogram production batch, isolating **1-HBr** in 88% yield and >99 wt% purity. Surprisingly, a second production batch yielded an atypical reaction profile. This second production batch showed unusually high levels of cyanamide **3**, formed by alkylation of **2** with CNBr, in the supernatant after 48 hours (Figure 1).⁶

Figure 1: Cyanamide intermediate 3



Furthermore, this reaction typically proceeded to 95% conversion with the balance of the starting amine **2** in the supernatant at the end of the reaction. However, **2** was absent from the supernatant in the second production batch, and was instead observed in the isolated solid following filtration. Based on these observations, our initial hypothesis was that a new, poorly soluble, phase of amine **2** or its corresponding HBr salt had crystallized under the reaction conditions, causing the reaction progress to stall before typical conversions could be achieved. To assess the validity of this hypothesis, the material isolated from the 2nd production batch was rigorously characterized to confirm the composition of the isolated solid.

Characterization of Isolated Solid from the 2nd Production Batch:

The HBr salts of **2** and **1** were known to exist as a crystalline acetonitrile solvate and an unsolvated phase, respectively. X-ray powder diffraction (XRPD) analysis on the solid from the 2nd production batch showed a mixture consisting of the desired phase of **1-HBr** and another unknown phase which was not similar to the **2-HBr** salt acetonitrile solvate (Figure 2).

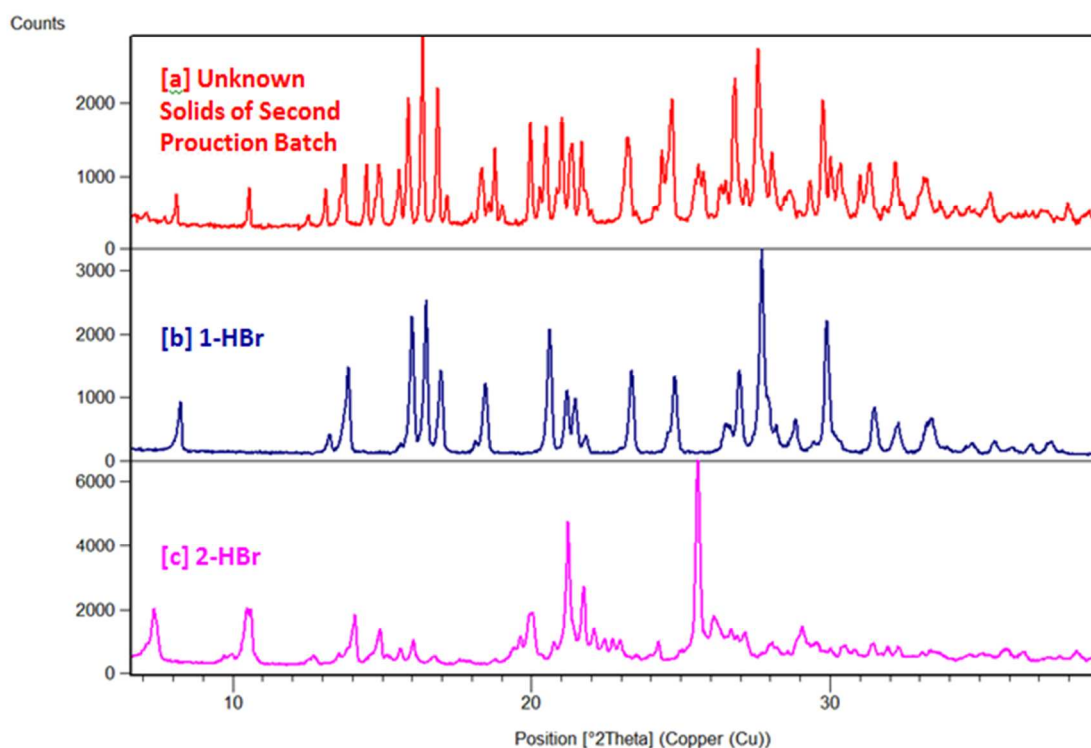


FIGURE 2: XRPD patterns of the unknown solids from the 2nd production batch solid ([a] red), the desired **1-HBr** Salt ([b] blue) and the **2-HBr**-acetonitrile solvate ([c] pink).

Scanning electron microscopy (SEM) analysis on the isolated solid (Figure 3a) indicated that two distinct morphologies were present in the powder; smaller particles with a block-like morphology (Figure 3b) (consistent with the previous batches of **1-HBr**) and larger aggregates

with a granule-like morphology. The observed size differential was exploited to physically separate the larger granules from the smaller particles by sieving through a series of screen sizes. Preliminary analysis of the smaller, block-like particles by single crystal diffraction gave unit cell dimensions consistent with the known desired anhydrate of **1-HBr**. XRPD analysis on the larger diameter sieve cut showed that this powder had been enriched in the new phase from the mixture with only minor amounts of **1-HBr** present. Utilizing the observed differential solubility of the unknown phase and **1-HBr**, the partially purified sieved aggregates were purified further by slurrying in acetonitrile (Figure 3c), with the resulting product essentially free of the known anhydrous phase of **1-HBr** (Figure 4). This separation/purification step significantly improved the ability to fully characterize the unknown solid isolated from the 2nd production batch.

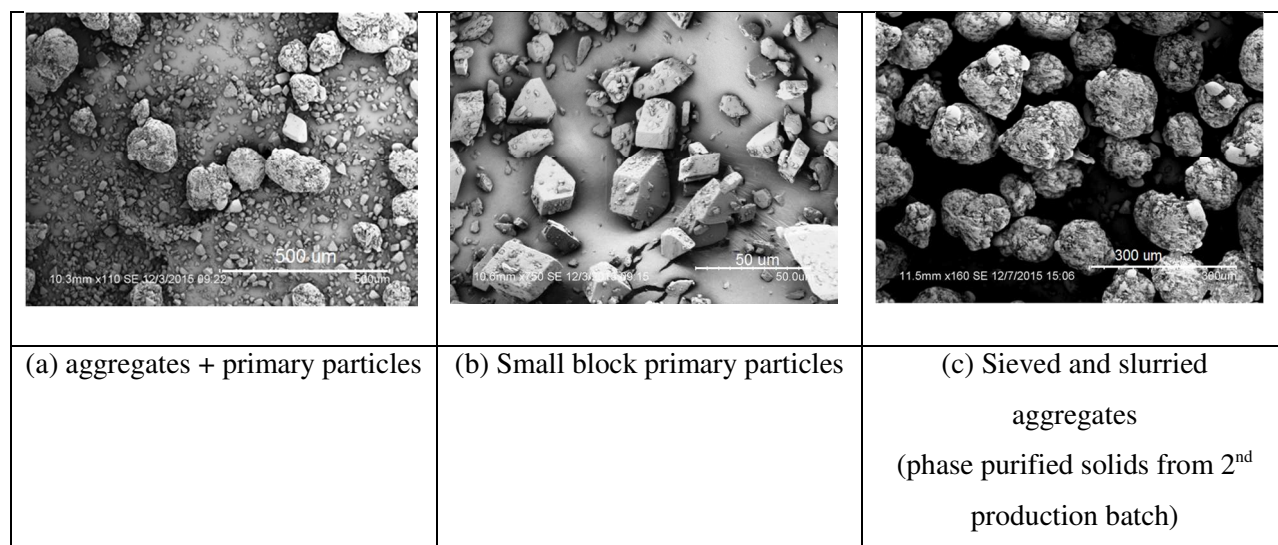


Figure 3: SEM images of solids from second production batch showing two distinct morphologies.

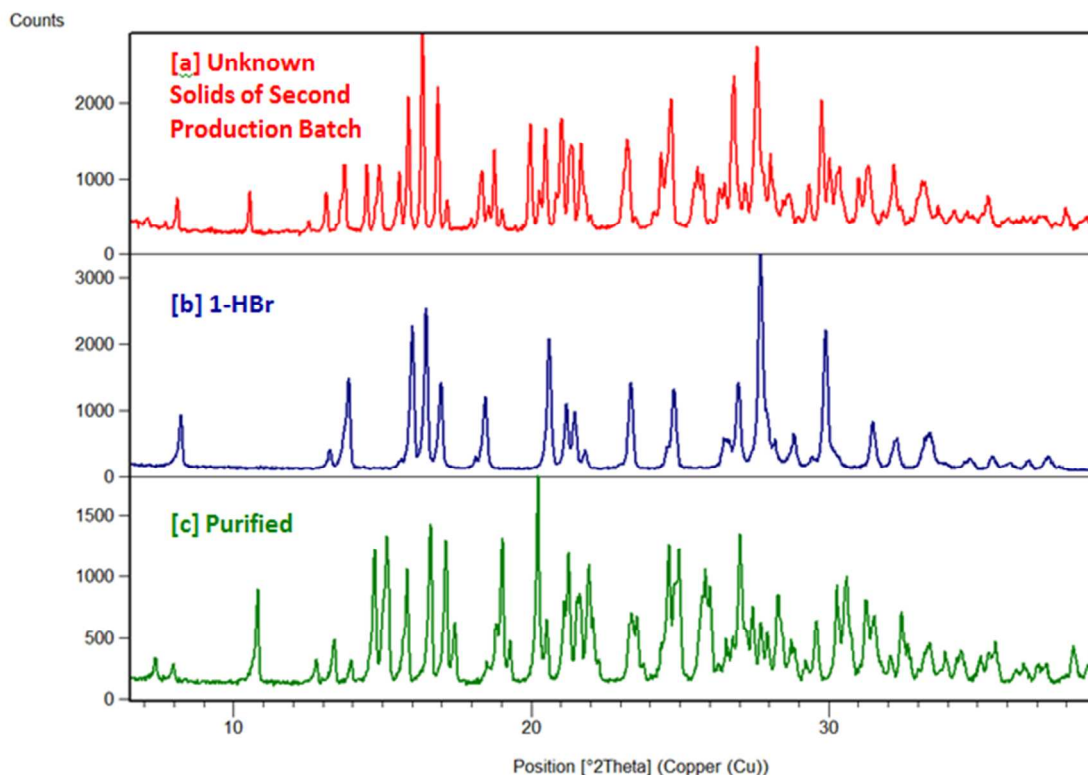


Figure 4: XRPD comparison of unknown solid from the 2nd production batch ([a]- red), **1-HBr** ([b]- blue), and the purified granule-like solids from the second production batch reaction ([c] – green)

To confirm the phase purity of the unknown phase, the unit cell was determined utilizing powder indexing. The indexing solution gave a monoclinic unit cell and space group $P2_1$, with no additional peaks that would be attributable to any other phases. The refined unit cell dimensions are shown in Table 1 and the Pawley fit is shown in Figure 5. The expected cell volume for a given crystal form and chemical species can be readily estimated by an atom additive approach by considering the likely number of molecules in the crystal form and its asymmetric unit.⁷ The estimated unit cell volumes for **2-HBr** and **1-HBr** are given in Table 2. For **2-HBr** and **1-HBr** the unit cell volume for the unknown phase would require $Z' = 2$ with two crystallographically

1
2
3 distinct copies of the salt in the crystal form. The unit cell volume was also consistent with a
4
5 crystal form where both salts were present in the asymmetric unit. Given that the phase was now
6
7 deemed to be phase pure, the sample was evaluated by thermal analysis as well as HPLC and
8
9 ICP-MS to determine the identity of the chemical species present.
10
11
12

13 Table 1: Unit cell of Unknown Phase by Powder Indexing and Pawley Refinement
14
15

<i>Crystal form</i>		<i>Unknown Phase</i>
Data Type / Temperature		PXRD / 293K
Crystal system, space group		Monoclinic, P2 ₁
Cell dimensions	<i>a</i> (Å)	7.03298
	<i>b</i> (Å)	22.60163
	<i>c</i> (Å)	12.28665
	α (°)	90
	β (°)	94.56598
	γ (°)	90
Cell Volume (Å ³)		1946.85

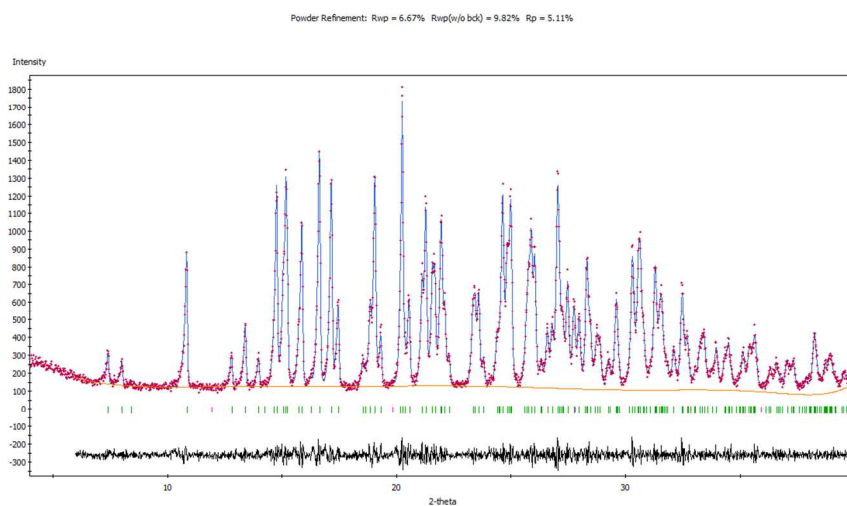


Figure 5: Pawley Fit of XRPD Pattern for Unknown Phase

Table 2: Estimated Cell Volumes (RT) for possible salts.

Chemical Species	Formula	Estimated Molecular Volume (\AA^3)	Z'/Z	Cell Volume (\AA^3)
2-HBr salt	C ₁₆ H ₁₉ Br ₁ F ₂ N ₄ O ₃ S ₁	480.1	2/4	1920.2
1-HBr	C ₁₇ H ₁₈ Br ₁ F ₂ N ₅ O ₃ S ₁	500.6	2/4	2002.5
2-HBr:1-HBr co-crystal	C ₃₃ H ₃₇ Br ₂ F ₄ N ₉ O ₆ S ₂	980.7	1/2	1961.4

HPLC and ICP-MS revealed the purified granules were a mixture of amine **2**, verbucastat **1** and two equivalents of HBr (Table 3). This analysis, showing an approximate 1:1:2 molar mixture of **2**:**1**:HBr, was consistent with the unknown phase that crystallized during the second production batch being a co-crystal of the HBr salts of both **2** and the desired product **1** (Figure 6). Co-crystals historically have been utilized in the pharmaceutical industry to improve solubility of drug substances and typically exist between the active molecule and a co-former⁸. Rarer instances exist between the molecular entity as a salt and a neutral co-former in the lattice⁹. The co-crystal discussed here is unique in that it formed between a salt of a reactant and a salt of the product.

Table 3: Component Analysis of Phase Purified Solids from the 2nd production batch.

Component	Wt % Found in impurity phase	Mole % of component	Mol % normalized to 1
Amine 2	40.1	23.6	1.01
verubecestat 1	42.4	23.5	1.00

HBr	18.6	52.8	2.25
-----	------	------	------

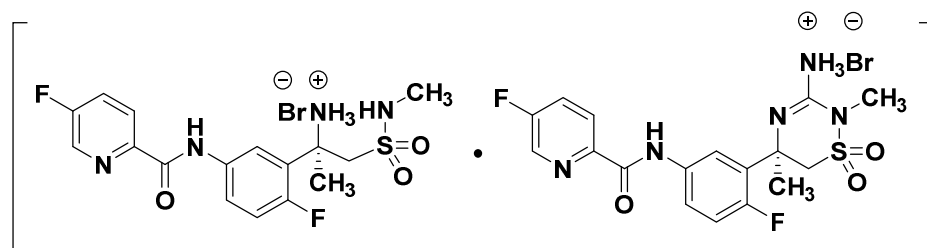


Figure 6: Co-crystal from the 2nd production batch

To further support this unprecedented finding, single crystal X-ray diffraction (SC-XRD) analysis on a sample of this purified phase was performed. The single crystal was obtained from acetonitrile by slow cooling of a saturated solution.. The single crystal unit cell dimensions are given in Table 4 along with the powder indexing cell dimensions for comparison. The cell dimensions are the same allowing for the cell contraction during the SC-XRD experiment, which was performed at 100K.

Table 4: Unit Cell Information for *2-HBr: 1-HBr*

<i>Crystal form</i>	<i>2-HBr: 1-HBr</i>	<i>2-HBr: 1-HBr</i>
Molecular Formula	C ₁₆ H ₁₈ F ₂ N ₄ O ₃ S · HBr : C ₁₇ H ₁₇ F ₂ N ₅ O ₃ S · HBr	C ₁₆ H ₁₈ F ₂ N ₄ O ₃ S · HBr : C ₁₇ H ₁₇ F ₂ N ₅ O ₃ S · HBr
Formula Weight	955.6	955.6
Data Type / Temperature	PXRD / 293K	SC-XRD / 100K

Crystal system, space group		Monoclinic, P2 ₁	Monoclinic, P2 ₁
Cell dimensions	<i>a</i> (Å)	7.0330	6.9896
	<i>b</i> (Å)	22.602	22.398
	<i>c</i> (Å)	12.2867	12.1743
	α (°)	90	90
	β (°)	94.566	94.093
	γ (°)	90	90
Cell Volume (Å ³)		1946.9	1901.1
<i>Z</i> (number of molecules per cell), <i>Z'</i> (number of molecules per asymmetric unit)		2,1	2,1
Crystal Density (g/cm ³)		1.630	1.669

SC-XRD confirmed the results of the component analysis. Figure 7a shows a thermal ellipsoid representation of the asymmetric unit contents consisting of the protonated amine-**2**, the protonated verubecestat-**1** and two bromide anions. Figure 7b shows the interactions to the bromide ions with the two organic moieties. One bromide interacts with both the protons of the endo and exocyclic nitrogens of protonated **1**, the protonated amine of **2** and the sulfonamide proton of another crystallographically distinct molecule of **2** (**Figure 7b, Br1Q**). The other bromide interacts with the amide proton of **2** and the exocyclic nitrogen proton of **1** (**Figure 7b, Br1R**).

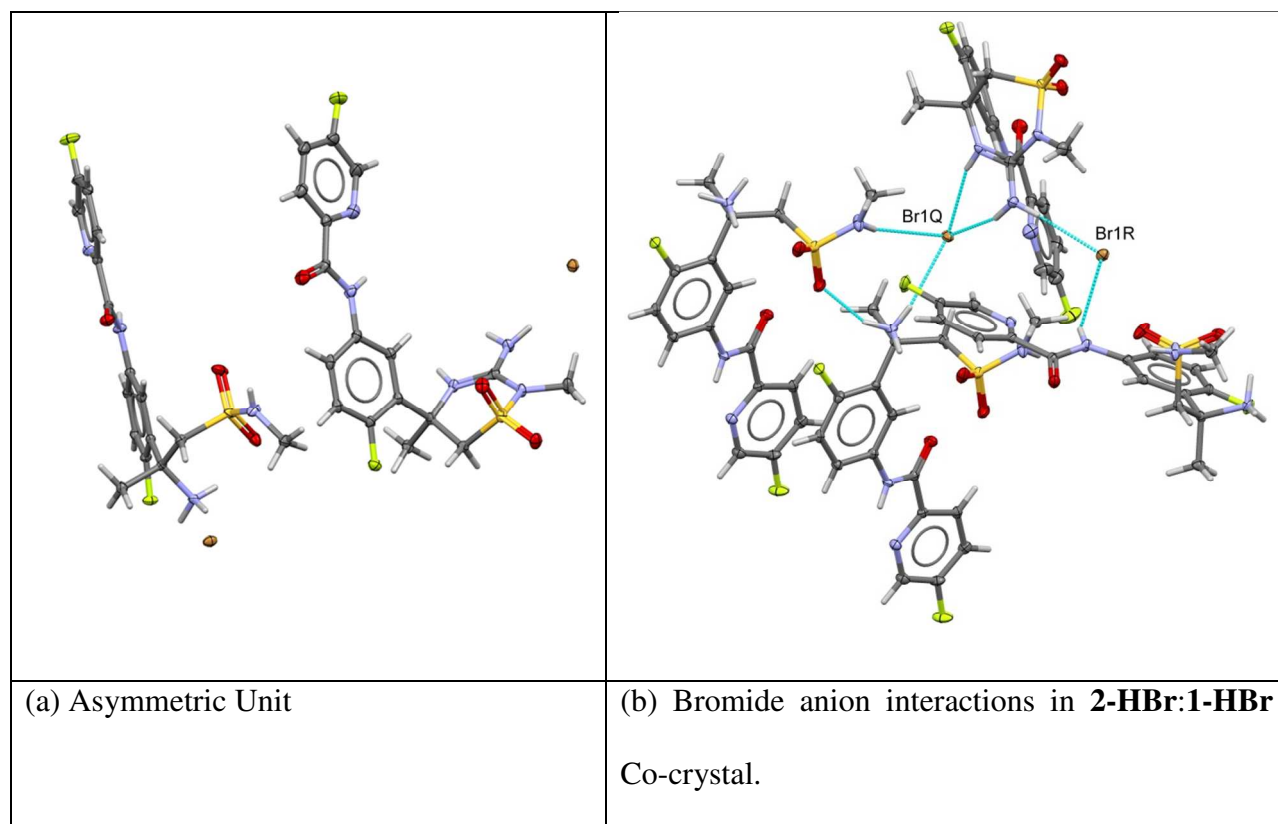


Figure 7: Single-crystal X-ray diffraction (SC-XRD) of the co-crystal formed between the HBr salt of **2** and **1**. Thermal ellipsoids are shown at the 50% probability level.

Solubility Assessment:

Single solubility measurements of the three solids (**2-HBr** MeCN solvate, **1-HBr**, and the co-crystal) were determined in the reaction solvent mixture at 70°C (Figure 8 and Table 5)

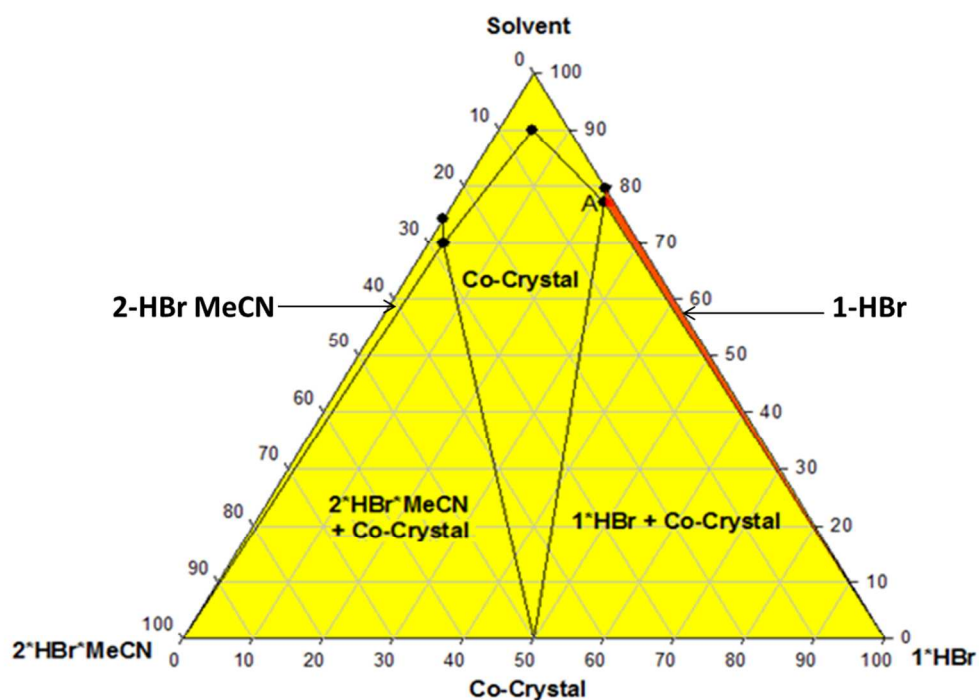


Figure 8: Pictorial representation for the ternary phase diagram of **2-HBr** MeCN solvate, **1-HBr**, co-crystal and reaction solvent mixture (not drawn to scale).

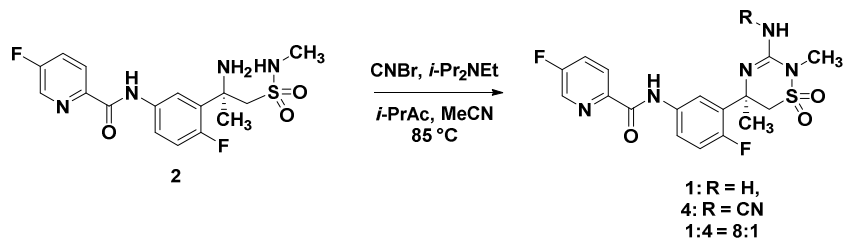
Table 5: Solubility Data for **2-HBr** MeCN solvate, **1-HBr** and the co-crystal

Phases in contact with solvent	Solution Composition of each Component at 25C (mg/g solution)		Solution Composition of each Component at 75C (mg/g solution)	
	2-HBr	2.44	-	21.0
2-HBr + Co-Crystal-HBr	2.35	0.029	21.9	0.153
Co-Crystal-HBr	0.155	0.171	0.487	0.521
1-HBr + Co-Crystal-HBr	0.063	1.06	0.219	2.79
1-HBr	-	1.05	-	2.58

In order to approach full conversion, the reactive crystallization would need to be performed in the region of the phase diagram where there is little or no co-crystal (**2-HBr**) out of solution. On the phase diagram, this is the far right triangular region bound by the **1-HBr** solid apex, the ternary solution point A, and the right leg of the phase diagram. The data shows that the region of the phase diagram where the reactive crystallization can be successfully executed is extremely limited. Furthermore, the crystallization of the co-crystal, slows down the reaction to an unacceptable rate providing insight to the mechanism of the reaction. The presence of cyanamide **3** in the supernatant of the second production batch coupled with the structural confirmation of the co-crystal formation provides support that soluble HBr is critical to promote the formation of the 3-amino-1,2,4-thiadiazinene 1,1'-dioxide heterocycle of **1** from **3**. Indeed, when **3** is treated with HBr in MeCN/IPAc, **1-HBr** is readily formed.

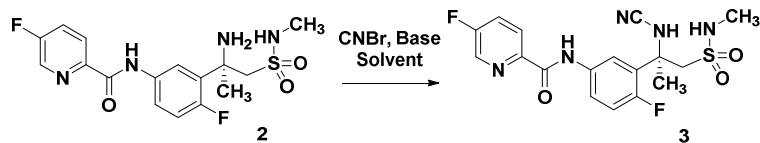
The low solubility of the co-crystal and the limited experimental operating range for which the reactive crystallization is viable rendered the existing end game chemistry untenable for future production campaigns. Our initial revision to the end game involved running the reaction under basic conditions in order to prevent the formation of the HBr salt of **2** and subsequent co-crystal formation. While this approach did generate **1**, the cyanation of the product in the presence of soluble organic bases such as *N,N*-diisopropylethylamine led to over-cyanated impurity **4** (Scheme 2) limiting the overall yield of the reaction.

Scheme 2: Conversion of **2** to **1** under basic reaction conditions



1
2
3 This result led us to consider a staged approach whereby **2** would first be converted
4 chemoselectively to cyanamide **3** before quenching the residual CNBr and promoting
5 intramolecular cyclization in a subsequent operation. Towards that end, amine bases weaker than
6
7
8
9
10 *N,N*-diisopropylethylamine provided **3** as the exclusive product, but in only 50-63% conversion
11 (Table 6, entries 1-3). Conversions improved using inorganic bases such as KH_2PO_4 or NaHCO_3 ,
12 which provided higher levels of **3** in a range of solvents (Table 6, entries 5, 6, 11, and 12). We
13
14
15 chose to optimize the reaction with NaHCO_3 rather than KH_2PO_4 , as the latter presented handling
16
17
18
19 challenges on scale due to its hygroscopicity. Some product decomposition was observed under
20
21
22 extended reaction times in MeOH or DMAc when using NaHCO_3 (Table 6, entries 8 and 9).
23
24 However, NMP, THF and 2-Me-THF were differentiated with respect to conversion and stream
25
26
27 stability, and high levels of conversion were achieved using 2-MeTHF when the process was
28
29
30 conducted at 45 °C. After full conversion to **3**, the stream was washed with aqueous sodium
31
32
33 thiosulfate which served to reduce residual CNBr (Scheme 3). The resulting 2-MeTHF stream
34
35
36 containing **3** was treated with aqueous sodium hydroxide to promote intramolecular cyclization
37
38
39 to **1**, accompanied by only trace amounts of over-cyanated **4**. Verubecestat **1** was isolated as its
40
41
42 *para*-toluenesulfonate salt (**1-pTSA**) for purity upgrade before performing a salt break with
43
44
45 potassium carbonate to afford **1** in 92% isolated yield from **2**.
46
47
48
49
50
51
52
53
54
55
56
57
58
59
60

Table 6: Solvent/Base Screen for the conversion of **2** to **3**

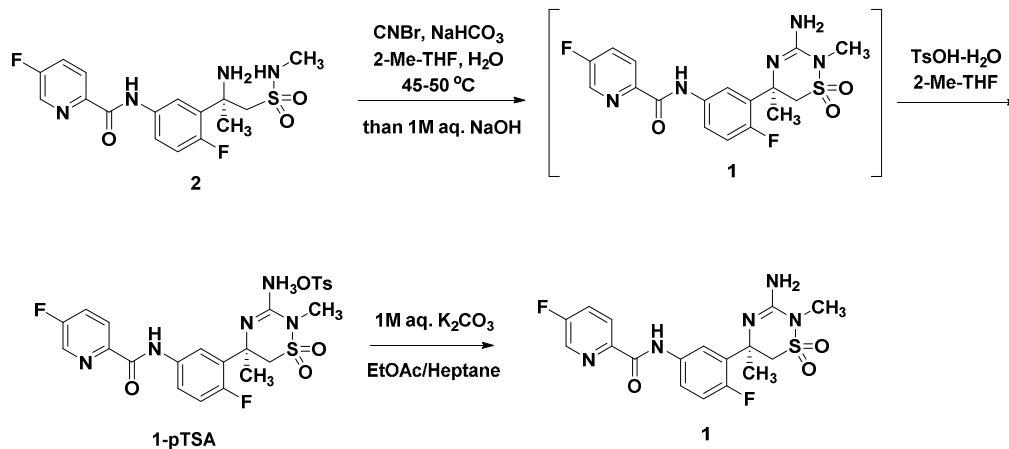


entry	solvent	base	% con. ^{a,b}
1	MeCN	HMDS	50
2	MeCN	Diethylaniline	56
3	MeCN	2,6-di-tert-butylpyridine	63
4	THF	K_2HPO_4	58
5	DMAc	K_2HPO_4	73
6	2-propanol	K_2HPO_4	86
7	NMP	K_2HPO_4	60
8	MeOH	NaHCO_3	63 (54)
9	DMAc	NaHCO_3	80 (71)
10	THF	NaHCO_3	53 (86)
11	NMP	NaHCO_3	96
12	2-Me-THF	NaHCO_3	> 99 ^c

^aDetermined by HPLC analysis after 24 h. ^bValues in parentheses refer to conversion

determined after 48 h. ^cReaction conducted at 45 °C.

Scheme 3: Preparation of verubecestat from **2**



Conclusion:

We have described the unexpected formation and subsequent characterization of an unprecedented crystalline intermediate identified during production scale manufacture of the

1
2
3 BACE1 inhibitor verubecestat (**1**). Rigorous physical characterization, including single crystal x-
4 ray analysis confirmed the structure of this unique intermediate and enabled the design of a
5 revised end game chemistry to prevent its formation. This new end game relied on a
6 chemoselective alkylation followed by intramolecular cyclization to furnish the 3-amino-1,2,4-
7 thiadiazinene 1,1'-dioxide heterocycle of **1**. This new end game has been demonstrated on
8 production scale and has provided robust access this potential disease modifying therapy.
9
10
11
12
13
14
15
16
17
18
19
20

21 **Author Information:**

22
23
24 Corresponding Authors

25
26
27 *E-mail: laura_artino@merck.com
28
29

30 **Notes:**

31
32
33 The authors declare no competing financial interest.
34
35

36 ASSOCIATED CONTENT

37
38
39 The process description, NMR data, single crystal data, Pawley refinement and analytical
40 methods descriptions for HPLC, ICP-MS, DSC and DSC data are available in the supporting
41 information section. This material is available free of charge via the Internet at
42 <http://pubs.acs.org>.
43
44
45
46
47

48 **Acknowledgements:**

49
50
51 The authors would like to thank Xiaodong Bu, Samreen Bano, Qiang Tu, Eric Regalado and Li
52 Zhang
53
54
55
56
57
58
59
60

References:

1. Alzheimer's Association. 2017 Alzheimer's Disease Facts and Figures. *Alzheimers Dementia* **2017**, *13*, 325-373.
2. Alzheimer's Disease International. World Alzheimer Report 2016.
3. Scott, J. D.; Li, S.W.; Brunskill, A. P. J.; Chen, X.; Cox, K.; Cumming, J. N.; Forman, M.; Gilbert, E. J.; Hodgson, R. A.; Hyde, L. A.; Jiang, Q.; Iserloh, U.; Kazakevich, I.; Kuvelkar, R.; Mei, H.; Meredith, J.; Misiaszek, J.; Orth, P.; Rossiter, L.M.; Slater, M.; Stone, J.; Strickland, C.; Voigt, J. H.; Wang, G.; Wang, H.; Wu, Y.; Greenlee, W. J.; Parker, E. M.; Kennedy, M. E.; Stamford, A. W. *J. Med. Chem.* **2016**, *59*, 10435–10450.
4. Kennedy, M. E.; Stamford, A. W.; Chen, X.; Cox, K.; Cumming, J. N.; Dockendorf, M. F.; Egan, M.; Ersehefsky, L.; Hodgson, R. A.; Hyde, L. A.; Jhee, S.; Kleijn, H. J.; Kuvelkar, R.; Li, W.; Mattson, B. A.; Mei, H.; Palcza, J.; Scott, J. D.; Tanen, M.; Troyer, M. D.; Tseng, J. L.; Stone, J. A.; Parker, E. M.; Forman, M. S. *Sci. Transl. Med.* **2016**, *8*, 363ra150.
5. Thaisrivongs, D. A.; Miller, S. P.; Molinaro, C.; Chen, Q.; Song, Z. J.; Tan, L.; Chen, L.; Chen, W.; Lekhal, A.; Pulicare, S. K.; Xu, Y. *Org. Lett.*, **2016**, *18*, 5780–5783.
6. The 2nd production batch showed >43% LCAP of cyanamide **3** present in the supernatant at the end of the reaction versus <1% LCAP expected.
7. Maguire, C. K.; Brunskill, A. P. J. *Mol. Pharmaceutics*, **2015**, *12*, 2061–2067.
8. Shan N, Zaworotko MJ. *Drug Discovery Today*, **2008**, *13*, 440–446.
9. Childs S.L.; Chyall L.J.; Dunlap J.T.; Smolenskaya V.N.; Stahly B.C.; Stahly G.P. *J. Am. Chem. Soc.*, **2004**, *126*, 13335-13342.